Inorganic Chemistry

pubs.acs.org/IC

Article

Diverse Thermal Expansion Behaviors in Ferromagnetic $Cr_{1-\delta}Te$ with NiAs-Type, Defective Structures

Chen Li, Ke Liu, Dequan Jiang, Cheng Jin, Tianyao Pei, Ting Wen, Binbin Yue, and Yonggang Wang*

Cite This: *Inorg. Chem.* 2022, 61, 14641−14647

Read Online

ACCESS | Metrics & More | Article Recommendations | Supporting Information

ABSTRACT: Negative thermal expansion (NTE) and zero thermal expansion (ZTE) properties are of great significance for the long-life stable operation of precision equipment. However, there are still existing challenges in finding new materials that exhibit NTE or ZTE over a wide temperature range. Here, we report negative, zero, and positive thermal expansion in NiAs-type, defective $Cr_{1-\delta}Te$, containing three compounds: hexagonal CrTe, monoclinic Cr_3Te_4, and trigonal Cr_5Te_8. CrTe shows the NTE behavior from 280 to 340 K with the volume coefficient of thermal expansion $\alpha_V = -27.6 \times 10^{-6}$ K^{-1}. Cr_3Te_4 shows the ZTE behavior over a wide temperature range of 180−320 K ($\alpha_V = 0.16 \times 10^{-6}$ K^{-1}). And Cr_5Te_8 holds the PTE behavior over the whole temperature range ($\alpha_V = 38.5 \times 10^{-6}$ K^{-1}). All of the samples show obvious anisotropic thermal expansion on heating. Combined with the magnetic measurements, it can be confirmed that the NTE and ZTE properties in ferromagnetic $Cr_{1-\delta}Te$ originate from the magnetovolume effect (MVE). Such NiAs-type, defective compounds with similar compositions but different structures provide a new perspective for tuning the NTE properties of materials and searching for new materials with ZTE over a wide temperature range.

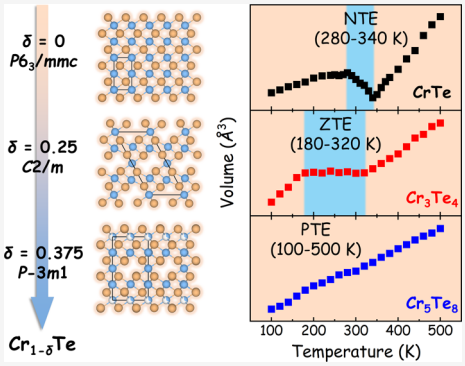

INTRODUCTION

Generally, most solid materials will exhibit length or volume expansion due to the increase of average interatomic distance on heating, that is, positive thermal expansion (PTE). However, there is a part of materials that decreases or is approximately constant in length or volume with increasing temperature, which is negative thermal expansion (NTE) and zero thermal expansion (ZTE). The thermal expansion of materials can be quantitatively characterized by the coefficient of thermal expansion (CTE).[1] NTE and ZTE behaviors have received extensive research interest due to the great significance for the stable and long-life operation of high-performance devices.[2−6] Besides, NTE materials have also been used as fluorescent host lattices in recent years to suppress thermal quenching and enhance luminescence.[7−9] NTE can be induced by various mechanisms, such as transversal vibration of bridged atoms for ZrW_2O_8,[10] spontaneous volume ferroelectrostriction for $PbTiO_3$-family,[11,12] the magnetovolume effect (MVE) for antiperovskite Mn_3GaN-family,[13,14] and charge transfer for $LaCu_3Fe_4O_{12}$.[15] These mechanisms provide guidelines for tailoring the NTE or ZTE behavior of materials. It is urgent to find those with large negative or zero CTE over a wide temperature range.

$Cr_{1-\delta}Te$ is a series of NiAs-type, defective ferromagnetic compounds with periodic vacancies. Depending on the vacancy concentration (δ), the crystal structures and magnetic properties of $Cr_{1-\delta}Te$ vary greatly.[16,17] The vacancies and vacancy concentrations mentioned in such structures are often specific to the hexagonal NiAs-type structure. CrTe ($\delta = 0$) crystallizes in hexagonal space group under ambient conditions, while Cr_3Te_4 ($\delta = 0.25$) and Cr_2Te_3 ($\delta = 0.333$) crystallize in monoclinic and trigonal space groups, respectively. Due to the slight difference in Te content, Cr_5Te_8 ($\delta = 0.375$) has monoclinic and hexagonal phases.[18] Curie temperature can be reduced from 360 to 160 K with the increasing vacancy concentration (δ).[19] Among them, hexagonal CrTe has been reported to decrease in volume on heating near its Curie temperature.[20] By analyzing the relationship between NTE and magnetic properties in detail, it was found that NTE in CrTe originated from the magnetovolume effect.[21] Also, NTE temperature range can be expanded by replacing Te with Se. Since $Cr_{1-\delta}Te$ with different vacancy concentrations are all ferromagnetic compounds, it would be interesting to explore whether $Cr_{1-\delta}Te$ with other vacancy concentration (δ) also has NTE. These compounds with similar compositions and different structures provide an excellent platform for studying the structure−activity relationship of materials.

In this work, we prepared three $Cr_{1-\delta}Te$ compounds by solid-state synthesis, including hexagonal CrTe, monoclinic Cr_3Te_4 and trigonal Cr_5Te_8. Interestingly, as the vacancy

Received: May 26, 2022
Published: September 6, 2022

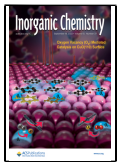

https://doi.org/10.1021/acs.inorgchem.2c01826
Inorg. Chem. 2022, 61, 14641−14647

concentration (δ) increases, their thermal expansion behaviors change from NTE in CrTe to ZTE in Cr_3Te_4 and then to PTE in Cr_5Te_8. Besides, all of the three compounds exhibited anisotropic thermal expansion upon cooling or heating. Combined with the analysis of variable-temperature X-ray diffraction (XRD) and magnetic measurements, it can be inferred that both NTE and ZTE in $Cr_{1-\delta}Te$ originate from the magnetovolume effect (MVE).

EXPERIMENTAL SECTION

Material Syntheses. Cr (Aladdin, 99.9%) and Te (Aladdin, 99.99%) powders with different stoichiometric amounts were thoroughly mixed in an argon-filled glovebox and then sealed into evacuated quartz tubes. After that, the tubes were heated at 800 °C for 2 days with intermediate grinding and reannealing to synthesize Cr_3Te_4 and Cr_5Te_8. For the synthesis of CrTe, the quartz tube containing raw materials was first heated at 1100 °C for 2 days with intermediate grinding and reannealing. After the obtained sample was thoroughly ground and reheated at 1200 °C for 40 min, it was cooled to 1100 °C slowly and then quenched to room temperature in cold water.

Characterizations. The phase purity was checked by powder X-ray diffraction (XRD) at room temperature using a PANalytical Empyrean diffractometer on Cu Kα radiation (λ = 1.5406 Å). The elemental composition was confirmed by energy-dispersive X-ray spectroscopy (EDS) attached to a JSM-7900F field emission scanning electron microscope (SEM). Raman spectra were recorded at room temperature using a Renishaw inVia reflex micro-Raman spectroscope with a 532 nm laser. X-ray photoelectron spectroscopy (XPS) was performed using a Thermo Fisher ESCALAB 250Xi photoelectron spectrometer with an Al Kα X-ray source. Binding energy is corrected using the C 1s peak fixed at 284.8 eV. Variable-temperature XRD patterns were collected using a Tongda TD-3700 diffractometer on Cu Kα radiation with a temperature control system. Magnetic properties were measured by a superconducting quantum interference device of quantum design with the vibrating sample magnetometer (SQUID-VSM). Structure refinements for all of the powder XRD patterns were performed using FullProf Suite software.[22]

RESULTS AND DISCUSSION

Syntheses and Crystal Structures of $Cr_{1-\delta}Te$. Three phase-pure compounds CrTe, Cr_3Te_4, and Cr_5Te_8 were obtained by direct high-temperature solid-state method. Figure 1 shows the powder XRD patterns of the as-obtained CrTe, Cr_3Te_4, and Cr_5Te_8, which can be well indexed in hexagonal $P6_3/mmc$ (ICSD #81719), monoclinic $C2/m$ (ICSD #626874), and trigonal $P\bar{3}m1$ (ICSD #50015), respectively. The refined parameters for CrTe are $a = b = 4.0048(1)$ Å and $c = 6.2402(3)$ Å with $R_p = 5.12\%$ and $R_{wp} = 6.65\%$. CrTe has a typical NiAs-type structure, which is composed of face-shared [$CrTe_6$] octahedra layers stacked along the c-axis to form a three-dimensional structure. For Cr_3Te_4, the refined parameters are $a = 13.9646(2)$ Å, $b = 3.9245(1)$ Å, $c = 6.8517(1)$ Å, and $\beta = 118.307(1)°$ with $R_p = 5.75\%$ and $R_{wp} = 7.09\%$. Compared with CrTe, the [$CrTe_6$] octahedra in Cr_3Te_4 are distorted, and periodic metal vacancies appear every two layers of atoms. Thus, the structure of Cr_3Te_4 can be considered as a $1 \times 2 \times 2$ supercell of the CrTe structure. For Cr_5Te_8, the refined parameters are $a = b = 7.7887(1)$ Å and $c = 11.9735(1)$ Å with $R_p = 6.22\%$ and $R_{wp} = 8.07\%$. It forms a $2 \times 2 \times 2$ supercell due to parts of Cr sites are not fully occupied besides periodic metal vacancies.

The elemental compositions of the as-synthesized CrTe, Cr_3Te_4, and Cr_5Te_8 samples are confirmed by EDS. As shown in Figure 2a, the elemental compositions of all samples are close to their respective chemical formulae. Notably, the synthesized CrTe is not in a perfect 1:1 stoichiometric ratio. It is reported that a certain amount of Cr vacancies in CrTe helps to hold the NiAs-type structure.[23] The results of EDS mapping show that the element distribution of the synthesized samples is relatively uniform (Figure S1). Despite sufficient grinding, there are still many flakes in CrTe and Cr_5Te_8, which leads to a certain preferred orientation in XRD. Raman spectra show that the three compounds have two distinct characteristic peaks with almost the same Raman shift, corresponding to the out-of-plane A_{1g} and in-plane E_g vibrational modes.[24] A_{1g} and E_g modes are often shared in the transition-metal chalcogenides crystallized in the trigonal or hexagonal system, corresponding to the atomic vibrations perpendicular to the ab plane and those in the ab plane, respectively.[25] Specifically, in CrTe and Cr_5Te_8, the two Raman peaks corresponding to A_{1g} and E_g are located at around 123 and 140 cm^{-1}, respectively. Due to the lattice distortion in Cr_3Te_4, the positions of Raman peaks slightly shift to 124 and 142 cm^{-1}, respectively. XPS spectra show that the positions of binding energy peaks of the three samples are almost the same, consistent with that reported by Shimada et al.[19] The peaks located at around 575.5 and 585.9 eV are attributed to Cr $2p_{2/3}$ and Cr $2p_{1/2}$, while those located at around 572.2 and 582.4 eV are attributed to Te $3d_{5/2}$ and Te $3d_{3/2}$, respectively. However, it is difficult to obtain reliable composition and valence information from XPS spectra as in the two-dimensional $Cr_{1-\delta}Te$ films.[24,26−29] It can just be observed that the Cr content of Cr_3Te_4 and Cr_5Te_8 is lower than that of CrTe. For Cr_3Te_4, Chua et al. assigned the two broad peaks at 572 and 582 eV to three components containing Te $3d_{5/2}$ (Te $3d_{3/2}$), Cr $2p_{3/2}$ (Cr $2p_{1/2}$), and Te from Te_xO_y,[26] but it seems to be more appropriate to assign them to different valence states of Cr instead of Te_xO_y.[30]

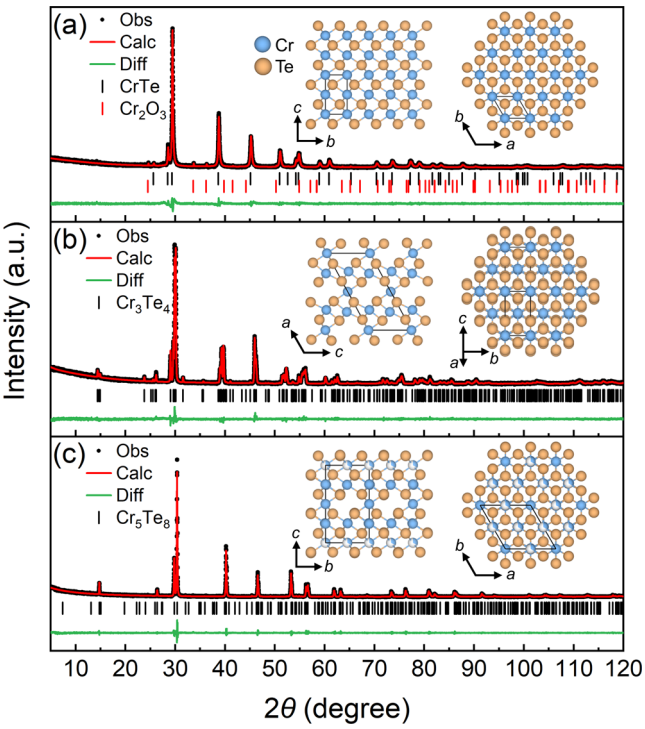

Figure 1. Structure refinements of powder XRD patterns for (a) CrTe (with a small amount of Cr_2O_3 impurity), (b) Cr_3Te_4, and (c) Cr_5Te_8. Inset: crystal structures of CrTe, Cr_3Te_4, and Cr_5Te_8 at room temperature.

https://doi.org/10.1021/acs.inorgchem.2c01826
Inorg. Chem. 2022, 61, 14641−14647

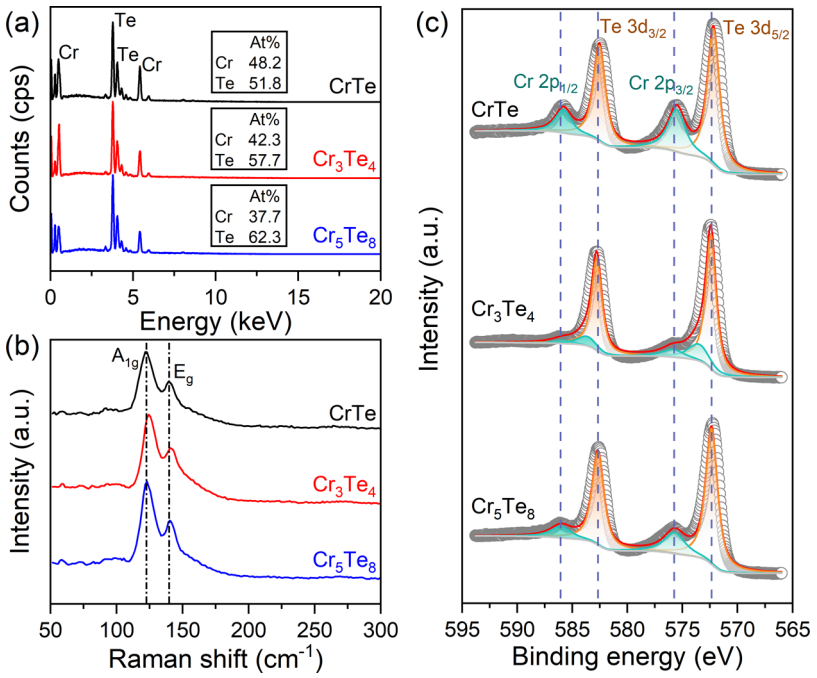

Figure 2. (a) EDS, (b) Raman, and (c) XPS spectra for CrTe, Cr_3Te_4, and Cr_5Te_8 at room temperature.

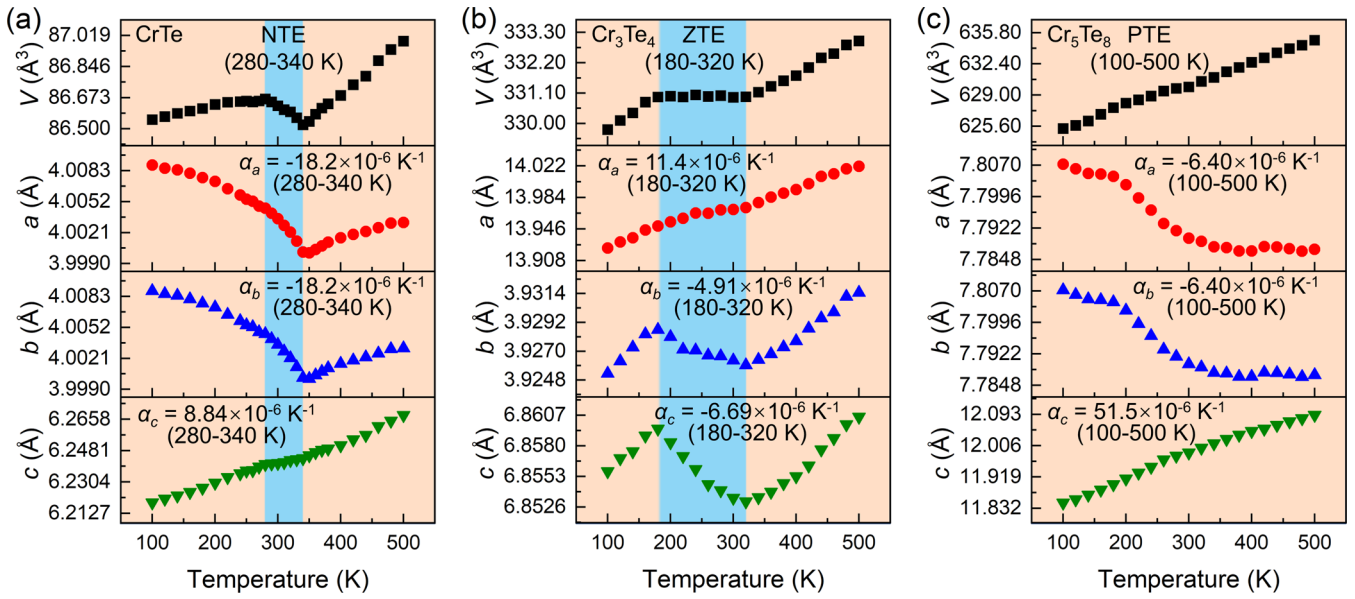

Figure 3. Temperature-dependent crystallographic parameters of (a) CrTe, (b) Cr_3Te_4, and (c) Cr_5Te_8. The blue ranges in (a) and (b) highlight the NTE and ZTE behaviors of CrTe and Cr_3Te_4.

NTE, ZTE, and PTE Properties of CrTe, Cr_3Te_4, and Cr_5Te_8. To explore the possible NTE properties of CrTe, Cr_3Te_4, and Cr_5Te_8, the as-obtained samples are characterized by variable-temperature XRD (Figure S2). By performing refinements for all of the XRD patterns at different temperatures, the temperature-dependent lattice crystallographic parameters of CrTe, Cr_3Te_4, and Cr_5Te_8 are shown in Figure 3. The results of refinements are partly shown in Figure S3. It can be obviously observed that CrTe shows the NTE behavior from 280 to 340 K, Cr_3Te_4 shows the ZTE behavior from 180 to 320 K, while Cr_5Te_8 shows the PTE behavior in the whole temperature range. Specifically, the thermal expansion coefficient of volume (α_V) of CrTe is -27.6×10^{-6} K^{-1} (280−340 K), close to that reported by Xu et al.[21] Correspondingly, the thermal expansion coefficients are calculated to be $\alpha_a = \alpha_b = -18.2 \times 10^{-6}$ K^{-1} and $\alpha_c = 8.84 \times 10^{-6}$ K^{-1} in the temperature range of 280−340 K, which indicated that the NTE behavior of CrTe origins from the shrink of the *a*-axis. In Cr_3Te_4, the β angle remains constant almost over the whole temperature range (Figure S4). The lattice parameters *b* and *c* decrease on heating from 180 to 320 K, while the lattice parameter *a* increases, resulting in that the unit cell volume of Cr_3Te_4 hardly changes from 180 to 320 K. The thermal expansion coefficients are $\alpha_V = 0.16 \times 10^{-6}$ K^{-1}, $\alpha_a = 11.4 \times 10^{-6}$ K^{-1}, $\alpha_b = -4.91 \times 10^{-6}$ K^{-1}, and $\alpha_c = -6.69 \times 10^{-6}$ K^{-1} in the temperature range of 180−320 K. Although the *a*-axis also shrinks on heating, due to the large elongation

https://doi.org/10.1021/acs.inorgchem.2c01826
Inorg. Chem. 2022, 61, 14641−14647

Table 1. Thermal Expansion Properties of CrTe, Cr_3Te_4, and Cr_5Te_8 in Selected Temperature Ranges

Sample	α_V/ × 10^{-6} K^{-1}	α_a/ × 10^{-6} K^{-1}	α_b/ × 10^{-6} K^{-1}	α_c/ × 10^{-6} K^{-1}	Temp. range/K
CrTe	−27.6	−18.2	−18.2	8.84	280−340
Cr_3Te_4	0.16	11.4	−4.91	−6.69	180−320
Cr_5Te_8	38.5	−6.40	−6.40	51.5	100−500

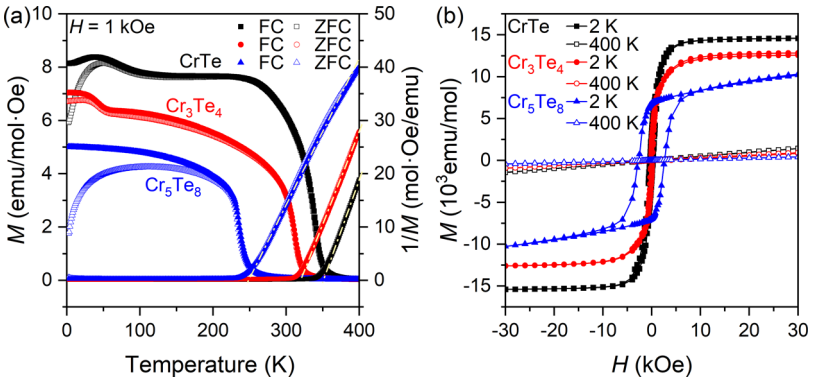

Figure 4. (a) Temperature-dependent magnetization (per mol Cr atom) for CrTe, Cr_3Te_4, and Cr_5Te_8 measured in the external magnetic field H = 1 kOe. The dashed lines are fitted by the modified Curie−Weiss law, and the fitted Weiss temperatures of CrTe, Cr_3Te_4, and Cr_5Te_8 are 351, 321, and 244 K, respectively. (b) Field-dependent magnetization for CrTe, Cr_3Te_4, and Cr_5Te_8 measured at 2 and 400 K.

of the c-axis, Cr_5Te_8 exhibits the PTE behavior in the whole temperature range (100−500 K).

All of the coefficients of thermal expansion (CTE) of CrTe, Cr_3Te_4, and Cr_5Te_8 are shown in Table 1. For all of the samples, the volume CTE is equal to the sum of the uniaxial CTE, *i.e.*, $\alpha_V = \alpha_a + \alpha_b + \alpha_c$. And all of the samples exhibit obvious anisotropic thermal expansion behaviors. With the increase of Cr vacancy concentration (δ), the thermal expansion coefficients of volume (α_V) of the samples change from a negative value to a near-zero value and up to a positive value finally. From the crystal structures of CrTe, Cr_3Te_4, and Cr_5Te_8, the heating leads to the shortening of the distance between atoms within the layers, while the normal thermal expansion law between the layers is maintained, which leads to the NTE behavior of CrTe and the ZTE behavior of Cr_3Te_4. Due to the existence of more vacancies, the NTE behavior within the layers is suppressed, while the PTE behavior between the layers is enhanced. This results in that the degree of uniaxial NTE of Cr_3Te_4 and Cr_5Te_8 is smaller than that of CrTe, while the PTE of c-axis in Cr_5Te_8 (α_c = 51.5 × 10^{-6} K^{-1}) is much larger than that in CrTe (α_c = 8.84 × 10^{-6} K^{-1}). From the obtained thermal expansion coefficients, the vacancy concentration (δ) has a strong impact on the thermal expansion behaviors of CrTe, Cr_3Te_4, and Cr_5Te_8. Not only that, but the magnetic properties of the system can also be greatly affected.

Magnetic Properties of CrTe, Cr_3Te_4, and Cr_5Te_8. As shown in Figure 4a, all of the three samples show obvious ferromagnetic (FM)-to-paramagnetic (PM) transitions during both of zero-field-cooling (ZFC) and field-cooling (FC) processes. For the sample of CrTe, since Cr_2O_3 is antiferromagnetic with a Neel temperature of about 318 K,[31] a small amount of Cr_2O_3 impurity has little effect on the measured magnetization. With the increase of vacancy concentration (δ), the Weiss temperature of CrTe, Cr_3Te_4, and Cr_5Te_8 gradually decreases, that is, 351 K for CrTe, 321 K for Cr_3Te_4, and 244 K for Cr_5Te_8. Since the Weiss molecular field near the transition temperature is not accurate enough, the transition temperature values obtained by fitting the Curie−Weiss law are slightly larger. According to the minimum of the derivative curve of the magnetization dM/dT (Figure S5), the Curie temperatures (T_c) of CrTe, Cr_3Te_4, and Cr_5Te_8 are determined to be 339, 313, and 235 K, respectively. Meanwhile, the magnetization of the samples also decreases with the increasing vacancy concentration (δ). Dijkstra et al. have reported that direct metal−metal interaction and Cr−Te covalency determine the magnitude of the moment on Cr atom in $Cr_{1-\delta}Te$.[32] It is found by band structure calculations that the Te 5p bands become magnetically polarized due to the strong Cr−Te covalent. The increase of vacancy concentration (δ) not only weakens the metal−metal interaction but also makes the Te polarization gradually change from positive to negative, resulting in a decrease in magnetization of CrTe, Cr_3Te_4, and Cr_5Te_8. Besides the obvious FM−PM transition, the obvious tuning points of magnetization from the ZFC and FC curves for CrTe and Cr_3Te_4 at 66 and 41 K can be attributed to the transitions from FM to canted antiferromagnetic (AFM) phases. Similar behaviors were also reported in single-crystalline Cr_4Te_5.[33] In Cr_5Te_8, a significant separation of ZFC and FC curves at low temperature indicates a strong magnetocrystalline anisotropy or the canting of spins of Cr.[34] This is consistent with the behaviors of Cr_5Te_8 single crystals and has been confirmed by neutron diffraction data.[35−37] From the M−H curves (Figure 4b), it is enough to saturate the magnetization of CrTe and Cr_3Te_4 under the magnetic field of H = 30 kOe. And the M−H curves show little hysteresis with the coercivity H_c = 0.28 kOe for CrTe and H_c = 0.15 kOe for Cr_3Te_4. In Cr_5Te_8, the coexistence between canted AFM and FM leads to an unsaturated magnetization at 2 K.[36] This also corresponds to the strong magnetocrystalline anisotropy in Cr_5Te_8, which results in a large hysteresis with the coercivity H_c = 2.73 kOe, much larger than that of CrTe and Cr_3Te_4. These results from M−H curves can be corroborated with the temperature-dependent magnetization for CrTe, Cr_3Te_4, and Cr_5Te_8.

Magnetovolume Effect (MVE) Responsible for the NTE/ZTE Behaviors in CrTe, Cr_3Te_4, and Cr_5Te_8. By the analysis of the results of the magnetic measurements for the

https://doi.org/10.1021/acs.inorgchem.2c01826
Inorg. Chem. 2022, 61, 14641−14647

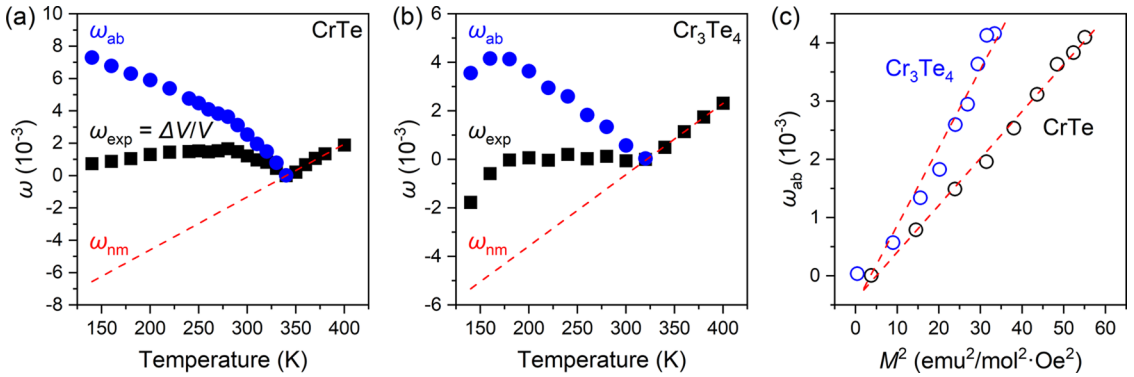

Figure 5. Temperature-dependent ω_{ab}, ω_{exp}, and ω_{nm} for (a) CrTe and (b) Cr_3Te_4. (c) Linear relationships between ω_{ab} and M^2.

samples, the temperatures at which the NTE and ZTE behaviors disappear correspond to the Curie temperature T_c = 339 K for CrTe and T_c = 313 K for Cr_3Te_4. The weakening of the ferromagnetic interaction leads to a decrease in the interlayer atomic distance on heating, leading to the NTE and ZTE behaviors of CrTe, Cr_3Te_4, and Cr_5Te_8. Near T_c, the *a*-axes of CrTe and Cr_5Te_8 shrink rapidly, while the *b*- and *c*-axes of Cr_3Te_4 begin to shrink; in fact, they both represent a decrease in the atomic distance within the layers. It has been recently discovered that the relationship between the *a*-axis and magnetism stems from the strong mixed bond between the nearest-neighbor Cr and Te atoms in CrTe.[23,38,39] Notably, the *a*- and *b*-axes of Cr_5Te_8 are still slowly shortening above the Curie temperature, which may be due to the existence of disordered Cr vacancies in the *ab* plane that counteract the contribution of the increased atomic vibrational amplitude to thermal expansion on heating. The decrease of magnetization and disordered vacancies together lead to *a*-axis and *b*-axis exhibiting linear NTE behaviors almost over the full temperature range. Based on the above discussion, it can be inferred that the NTE and ZTE behaviors exhibited in CrTe, Cr_3Te_4, and Cr_5Te_8 are closely related to the magnetic transitions, more precisely, the magnetovolume effect (MVE).

Many magnetic materials have been found to exhibit NTE or ZTE behaviors originated from the MVE, such as the Invar alloys of Fe−Ni,[40] (Zr,Nb)Fe_2,[41] Tb(Co,Fe)$_2$,[42] and the antiperovskites $Mn_3(Zn, M)_xN$ (M = Ag, Ge).[43] To clearly reveal the relationship between NTE, ZTE, and magnetic properties in CrTe, Cr_3Te_4, and Cr_5Te_8, as shown in Figure 5a,b, we calculate the spontaneous volume magnetostriction (ω_{ab}) with the following formula

$$\omega_{ab} = \omega_{exp} - \omega_{nm} \quad (1)$$

where ω_{ab} is the contribution of MVE for the anomalous thermal expansion,[44,45] ω_{exp} is the experimental data from XRD, and ω_{nm} represents the normal thermal expansion obtained by fitting the data from the high-temperature range. Meanwhile, according to the MVE theory, ω_{ab} has the following relationship with the local magnetic moments

$$\omega_{ab} = kCM(T)^2 \quad (2)$$

where k is the compressibility, C is the magnetovolume coupling constant, and $M(T)$ represents the local magnetic moments as a function of temperature.[1,46−48] As shown in Figure 5c, a clear linear relationship is observed after using the magnetization to approximately replace the local magnetic moment, which also effectively indicates that the NTE and ZTE behaviors in CrTe and Cr_3Te_4 originate from MVE. When the contribution of MVE on the thermal expansion is larger than that of normal thermal expansion, the material exhibits the NTE behavior.

CONCLUSIONS

In summary, we report the NTE, ZTE, and PTE behaviors in NiAs-type, defective $Cr_{1-\delta}Te$ compounds CrTe, Cr_3Te_4, and Cr_5Te_8. Hexagonal CrTe shows the NTE behavior from 280 to 340 K with the volume coefficient of thermal expansion (α_V) of -27.6×10^{-6} K^{-1}. Monoclinic Cr_3Te_4 shows the ZTE behavior over a wide temperature range of 180−320 K with $\alpha_V = 0.16 \times 10^{-6}$ K^{-1}. While trigonal Cr_5Te_8 exhibits the PTE behavior over the full range from 100 to 500 K with $\alpha_V = 38.5 \times 10^{-6}$ K^{-1}. The presence of more vacancies in the system can suppress NTE within layers and enhance PTE between layers. Combined with the magnetic measurements of the samples, it can be inferred that the NTE and ZTE behaviors exhibited in ferromagnetic CrTe, Cr_3Te_4, and Cr_5Te_8 originate from MVE. The diverse thermal expansion behaviors of CrTe, Cr_3Te_4, and Cr_5Te_8 provide a new way to tune the NTE properties of the materials and find new wide-temperature-range ZTE materials.

ASSOCIATED CONTENT

Supporting Information

The Supporting Information is available free of charge at https://pubs.acs.org/doi/10.1021/acs.inorgchem.2c01826.

Element mapping images, variable-temperature XRD patterns, structure refinements, β angle of Cr_3Te_4 as a function of temperature, and derivative magnetization dM/dT as a function of temperature (PDF)

AUTHOR INFORMATION

Corresponding Author

Yonggang Wang − *Center for High Pressure Science and Technology Advanced Research (HPSTAR), Beijing 100193, China; School of Materials Science and Engineering, Peking University, Beijing 100871, China;* orcid.org/0000-0003-4816-9182; Email: yonggang.wang@hpstar.ac.cn

Authors

Chen Li − *Center for High Pressure Science and Technology Advanced Research (HPSTAR), Beijing 100193, China;* orcid.org/0000-0002-1563-6939

Ke Liu − *Center for High Pressure Science and Technology Advanced Research (HPSTAR), Beijing 100193, China*

Dequan Jiang − *Center for High Pressure Science and Technology Advanced Research (HPSTAR), Beijing 100193, China;* orcid.org/0000-0003-0998-5507
Cheng Jin − *Center for High Pressure Science and Technology Advanced Research (HPSTAR), Beijing 100193, China*
Tianyao Pei − *Center for High Pressure Science and Technology Advanced Research (HPSTAR), Beijing 100193, China*
Ting Wen − *Center for High Pressure Science and Technology Advanced Research (HPSTAR), Beijing 100193, China;* orcid.org/0000-0001-6572-0920
Binbin Yue − *Center for High Pressure Science and Technology Advanced Research (HPSTAR), Beijing 100193, China;* orcid.org/0000-0002-7784-2850

Complete contact information is available at: https://pubs.acs.org/10.1021/acs.inorgchem.2c01826

Notes

The authors declare no competing financial interest.

■ ACKNOWLEDGMENTS

This work was supported by the Major Program of the National Natural Science Foundation of China (22090041), the National Natural Science Foundation of China (52073003), and the National Key R&D Program of China (2018YFA0305900).

■ REFERENCES

(1) Chen, J.; Hu, L.; Deng, J.; Xing, X. Negative thermal expansion in functional materials: controllable thermal expansion by chemical modifications. *Chem. Soc. Rev.* **2015**, *44*, 3522−3567.
(2) Evans, J. S. O. Negative thermal expansion materials. *J. Chem. Soc., Dalton Trans.* **1999**, 3317−3326.
(3) Li, Q.; Lin, K.; Liu, Z.; Hu, L.; Cao, Y.; Chen, J.; Xing, X. Chemical diversity for tailoring negative thermal expansion. *Chem. Rev.* **2022**, *122*, 8438−8486.
(4) Coates, C. S.; Goodwin, A. L. How to quantify isotropic negative thermal expansion: magnitude, range, or both? *Mater. Horiz.* **2019**, *6*, 211−218.
(5) Liang, E.; Sun, Q.; Yuan, H.; Wang, J.; Zeng, G.; Gao, Q. Negative thermal expansion: Mechanisms and materials. *Front. Phys.* **2021**, *16*, 53302.
(6) Sun, Q.; Jin, K.; Huang, Y.; Guo, J.; Rungrotmongkol, T.; Maitarad, P.; Wang, C. Influence of conformational change of chain unit on the intrinsic negative thermal expansion of polymers. *Chin. Chem. Lett.* **2021**, *32*, 1515−1518.
(7) Xie, J.; Xie, X.; Mi, C.; Gao, Z.; Pan, Y.; Fan, Q.; Su, H.; Jin, D.; Huang, L.; Huang, W. Controlled synthesis, evolution mechanisms, and luminescent properties of ScF_x:Ln (x =2.76, 3) nanocrystals. *Chem. Mater.* **2017**, *29*, 9758−9766.
(8) Zou, H.; Yang, X.; Chen, B.; Du, Y.; Ren, B.; Sun, X.; Qiao, X.; Zhang, Q.; Wang, F. Thermal enhancement of upconversion by negative lattice expansion in orthorhombic $Yb_2W_3O_{12}$. *Angew. Chem., Int. Ed.* **2019**, *58*, 17255−17259.
(9) Liao, J.; Wang, M.; Lin, F.; Han, Z.; Fu, B.; Tu, D.; Chen, X.; Qiu, B.; Wen, H.-R. Thermally boosted upconversion and down-shifting luminescence in $Sc_2(MoO_4)_3$:Yb/Er with two-dimensional negative thermal expansion. *Nat. Commun.* **2022**, *13*, No. 2090.
(10) Mary, T. A.; Evans, J. S. O.; Vogt, T.; Sleight, A. W. Negative thermal expansion from 0.3 to 1050 kelvin in ZrW_2O_8. *Science* **1996**, *272*, 90−92.
(11) Chen, J.; Nittala, K.; Forrester, J. S.; Jones, J. L.; Deng, J.; Yu, R.; Xing, X. The role of spontaneous polarization in the negative thermal expansion of tetragonal $PbTiO_3$-based compounds. *J. Am. Chem. Soc.* **2011**, *133*, 11114−11117.
(12) Chen, J.; Fan, L.; Ren, Y.; Pan, Z.; Deng, J.; Yu, R.; Xing, X. Unusual transformation from strong negative to positive thermal expansion in $PbTiO_3$ − $BiFeO_3$ perovskite. *Phys. Rev. Lett.* **2013**, *110*, No. 115901.
(13) Deng, S.; Sun, Y.; Wu, H.; Huang, Q.; Yan, J.; Shi, K.; Malik, M. I.; Lu, H.; Wang, L.; Huang, R.; Li, L.; Wang, C. Invar-like behavior of antiperovskite $Mn_{3+x}Ni_{1-x}N$ compounds. *Chem. Mater.* **2015**, *27*, 2495−2501.
(14) Shi, K.; Sun, Y.; Yan, J.; Deng, S.; Wang, L.; Wu, H.; Hu, P.; Lu, H.; Malik, M. I.; Huang, Q.; Wang, C. Baromagnetic effect in antiperovskite $Mn_3Ga_{0.95}N_{0.94}$ by neutron powder diffraction analysis. *Adv. Mater.* **2016**, *28*, 3761−3767.
(15) Long, Y. W.; Hayashi, N.; Saito, T.; Azuma, M.; Muranaka, S.; Shimakawa, Y. Temperature-induced A-B intersite charge transfer in an A-site-ordered $LaCu_3Fe_4O_{12}$ perovskite. *Nature* **2009**, *458*, 60−63.
(16) Ipser, H.; Komarek, K. L.; Klepp, K. O. Transition metal-chalcogen systems VIII: The Cr-Te phase diagram. *J. Less-Common Met.* **1983**, *92*, 265−282.
(17) Chattopadhyay, G. The Cr-Te (chromium-tellurium) system. *J. Phase Equilib.* **1994**, *15*, 431−440.
(18) Bensch, W.; Helmer, O.; Näther, C. Determination and redetermination of the crystal structures of chromium tellurides in the composition range $CrTe_{1.56}$-$CrTe_{1.67}$: trigonal di-chromium tri-telluride Cr_2Te_3, monoclinic penta-chromium octa-telluride Cr_5Te_8, and the five layer superstructure of trigonal penta-chromium octa-telluride Cr_5Te_8. *Mater. Res. Bull.* **1997**, *32*, 305−318.
(19) Shimada, K.; Saitoh, T.; Namatame, H.; Fujimori, A.; et al. Photoemission study of itinerant ferromagnet $Cr_{1-\delta}Te$. *Phys. Rev. B* **1996**, *53*, 7673.
(20) Ohta, S.; Kanomata, T.; Kaneko, T.; Yoshida, H. Pressure effect on the Curie temperature and thermal expansion of CrTe. *J. Phys.: Condens. Matter* **1993**, *5*, 2759−2768.
(21) Xu, J.; Zheng, X.; Yang, S.; Xi, L.; Wang, S.; Zhang, L.; Yang, W.; Yang, J.; Ma, X.; Chen, D.; He, L.; Deng, S.; Zhang, J.; Wu, Y.; Shen, B. Large linear negative thermal expansion in NiAs-type magnetic intermetallic Cr-Te-Se compounds. *Inorg. Chem.* **2020**, *59*, 8603−8608.
(22) Rodríguez-Carvajal, J. Recent advances in magnetic structure determination by neutron powder diffraction. *Physica B Condens. Matter* **1993**, *192*, 55−69.
(23) Kanomata, T.; Suzuki, N.; Nishihara, H.; Kaneko, T.; Kato, H.; Fujii, N.; Ishizuka, M.; Endo, S. Low-temperature magnetic behavior of $Cr_{48}Te_{52}$. *Phys. B* **2000**, *284*−*288*, 1515−1516.
(24) Chen, C.; Chen, X.; Wu, C.; Wang, X.; Ping, Y.; Wei, X.; Zhou, X.; Lu, J.; Zhu, L.; Zhou, J.; Zhai, T.; Han, J.; Xu, H. Air-stable 2D Cr_5Te_8 nanosheets with thickness-tunable ferromagnetism. *Adv. Mater.* **2021**, *34*, No. 2107512.
(25) Hajiyev, P.; Cong, C.; Qiu, C.; Yu, T. Contrast and Raman spectroscopy study of single- and few-layered charge density wave material: 2H-$TaSe_2$. *Sci. Rep.* **2013**, *3*, No. 2593.
(26) Chua, R.; Zhou, J.; Yu, X.; Yu, W.; Gou, J.; Zhu, R.; Zhang, L.; Liu, M.; Breese, M. B. H.; Chen, W.; Loh, K. P.; Feng, Y. P.; Yang, M.; Huang, Y. L.; Wee, A. T. S. Room temperature ferromagnetism of monolayer chromium telluride with perpendicular magnetic anisotropy. *Adv. Mater.* **2021**, *33*, No. 2103360.
(27) Guo, Y.; Kang, L.; Yu, S.; Yang, J.; Qi, X.; Zhang, Z.; Liu, Z. CVD growth of large-scale and highly crystalline 2D chromium telluride nanoflakes. *ChemNanoMat* **2021**, *7*, 323−327.
(28) Tang, B.; Wang, X.; Han, M.; Xu, X.; Zhang, Z.; Zhu, C.; Cao, X.; Yang, Y.; Fu, Q.; Yang, J.; Li, X.; Gao, W.; Zhou, J.; Lin, J.; Liu, Z. Phase engineering of Cr_5Te_8 with colossal anomalous Hall effect. *Nat. Electron.* **2022**, *5*, 224−232.
(29) Bian, M.; Zhu, L.; Wang, X.; Choi, J.; Chopdekar, R. V.; Wei, S.; Wu, L.; Huai, C.; Marga, A.; Yang, Q.; Li, Y. C.; Yao, F.; Yu, T.; Crooker, S. A.; Cheng, X. M.; Sabirianov, R. F.; Zhang, S.; Lin, J.; Hou, Y.; Zeng, H. Dative epitaxy of commensurate monocrystalline covalent van der Waals Moiré supercrystal. *Adv. Mater.* **2022**, *34*, No. 2200117.

(30) Zhang, X.; Wang, B.; Guo, Y.; Zhang, Y.; Chen, Y.; Wang, J. High Curie temperature and intrinsic ferromagnetic half-metallicity in two-dimensional Cr_3X_4 (X = S, Se, Te) nanosheets. *Nanoscale Horiz.* **2019**, *4*, 859−866.
(31) Brockhouse, B. N. Antiferromagnetic structure in Cr_2O_3. *J. Chem. Phys.* **1953**, *21*, 961.
(32) Dijkstra, J.; Weitering, H. H.; van Bruggen, C. F.; Haas, C.; de Groot, R. A. Band-structure calculations, and magnetic and transport properties of ferromagnetic chromium tellurides (CrTe, Cr_3Te_4, Cr_2Te_3). *J. Phys.: Condens. Matter* **1989**, *1*, 9141−9161.
(33) Zhang, L.-Z.; Zhang, A.-L.; He, X.-D.; Ben, X.-W.; Xiao, Q.-L.; Lu, W.-L.; Chen, F.; Feng, Z.; Cao, S.; Zhang, J.; Ge, J.-Y. Critical behavior and magnetocaloric effect of the quasi-two-dimensional room-temperature ferromagnet Cr_4Te_5. *Phys. Rev. B* **2020**, *101*, No. 214413.
(34) Liu, Y.; Petrovic, C. Critical behavior of the quasi-two-dimensional weak itinerant ferromagnet trigonal chromium telluride $Cr_{0.62}Te$. *Phys. Rev. B* **2017**, *96*, No. 134410.
(35) Mondal, R.; Kulkarni, R.; Thamizhavel, A. Anisotropic magnetic properties and critical behavior studies of trigonal Cr_5Te_8 single crystal. *J. Magn. Magn. Mater.* **2019**, *483*, 27−33.
(36) Zhang, L.-Z.; He, X.-D.; Zhang, A.-L.; Xiao, Q.-L.; Lu, W.-L.; Chen, F.; Feng, Z.; Cao, S.; Zhang, J.; Ge, J.-Y. Tunable Curie temperature in layered ferromagnetic $Cr_{5+x}Te_8$ single crystals. *APL Mater.* **2020**, *8*, No. 031101.
(37) Huang, Z.-L.; Kockelmann, W.; Telling, M.; Bensch, W. A neutron diffraction study of structural and magnetic properties of monoclinic Cr_5Te_8. *Solid State Sci.* **2008**, *10*, 1099−1105.
(38) Polesya, S.; Mankovsky, S.; Benea, D.; Ebert, H.; Bensch, W. Finite-temperature magnetism of CrTe and CrSe. *J. Phys.: Condens. Matter* **2010**, *22*, No. 156002.
(39) Block, T.; Tremel, W. Large magnetoresistance at room temperature in the off-stochiometric chalcogenide $Cr_{0.92}Te$. *J. Alloys Compd.* **2006**, *422*, 12−15.
(40) van Schilfgaarde, M.; Abrikosov, I.; Johansson, B. Origin of the Invar effect in iron−nickel alloys. *Nature* **1999**, *400*, 46−49.
(41) Song, Y.; Sun, Q.; Yokoyama, T.; Zhu, H.; Li, Q.; Huang, R.; Ren, Y.; Huang, Q.; Xing, X.; Chen, J. Transforming thermal expansion from positive to negative: the case of cubic magnetic compounds of $(Zr,Nb)Fe_2$. *J. Phys. Chem. Lett.* **2020**, *11*, 1954−1961.
(42) Song, Y.; Chen, J.; Liu, X.; Wang, C.; Zhang, J.; Liu, H.; Zhu, H.; Hu, L.; Lin, K.; Zhang, S.; Xing, X. Zero thermal expansion in magnetic and metallic $Tb(Co,Fe)_2$ intermetallic compounds. *J. Am. Chem. Soc.* **2018**, *140*, 602−605.
(43) Wang, C.; Chu, L.; Yao, Q.; et al. Tuning the range, magnitude, and sign of the thermal expansion in intermetallic $Mn_3(Zn, M)_xN$ (*M* = Ag, Ge). *Phys. Rev. B: Condens. Matter Mater. Phys.* **2012**, *85*, No. 220103.
(44) Ibarra, M. R.; Algarabel, P. A.; Marquina, C.; Blasco, J.; García, J. Large magnetovolume effect in yttrium doped La-Ca-Mn-O perovskite. *Phys. Rev. Lett.* **1995**, *75*, 3541.
(45) Song, Y.; Shi, N.; Deng, S.; Xing, X.; Chen, J. Negative thermal expansion in magnetic materials. *Prog. Mater. Sci.* **2021**, *121*, No. 100835.
(46) Shi, K.; Sun, Y.; Colin, C. V.; Wang, L.; Yan, J.; Deng, S.; Lu, H.; Zhao, W.; Kazunari, Y.; Bordet, P.; Wang, C. Investigation of the spin-lattice coupling in $Mn_3Ga_{1-x}Sn_xN$ antiperovskites. *Phys. Rev. B* **2018**, *97*, No. 054110.
(47) Moriya, T.; Usami, K. Magneto-volume effect and invar phenomena in ferromagnetic metals. *Solid State Commun.* **1980**, *34*, 95−99.
(48) Fujita, A.; Fukamichi, K.; Wang, J.-T.; Kawazoe, Y. Large magnetovolume effects and band structure of itinerant-electron metamagnetic $La(Fe_xSi_{1-x})_{13}$ compounds. *Phys. Rev. B: Condens. Matter Mater. Phys.* **2003**, *68*, No. 104431.

https://doi.org/10.1021/acs.inorgchem.2c01826
Inorg. Chem. 2022, 61, 14641−14647